Petroleum Science 21 (2024) 765–776

Contents lists available at ScienceDirect

Petroleum Science

journal homepage: www.keaipublishing.com/en/journals/petroleum-science

Original Paper

Differences and identification on multi-time hydrocarbon generation of carboniferous-permian coaly source rocks in the Huanghua Depression, Bohai Bay Basin

Jin-Jun Xu [a], Xian-Gang Cheng [a], Shu-Nan Peng [a], Jun-Cai Jiang [a], Qi-Long Wu [a], Da Lou [b], Fu-Qi Cheng [a, *], La-Mei Lin [a]

[a] National Key Laboratory of Deep Oil and Gas, China University of Petroleum (East China), Qingdao 266580, Shandong, China
[b] PetroChina Dagang Oilfield Company, Tianjin, 300280, China

ARTICLE INFO

Article history:
Received 20 November 2022
Received in revised form
28 July 2023
Accepted 8 November 2023
Available online 13 November 2023

Edited by Jie Hao and Teng Zhu

Keywords:
Thermal simulation
Multi-time oil generation processes
Coaly source rock
Carboniferous-permian
Huanghua Depression

ABSTRACT

Coal is a solid combustible mineral, and coal-bearing strata have important hydrocarbon generation potential and contribute to more than 12% of the global hydrocarbon resources. However, the deposition and hydrocarbon evolution process of ancient coal-bearing strata is characterized by multiple geological times, leading to obvious distinctions in their hydrocarbon generation potential, geological processes, and production, which affect the evaluation and exploration of hydrocarbon resources derived from coaly source rocks worldwide. This study aimed to identify the differences on oil-generated parent macerals and the production of oil generated from different coaly source rocks and through different oil generation processes. Integrating with the analysis of previous tectonic burial history and hydrocarbon generation history, high-temperature and high-pressure thermal simulation experiments, organic geochemistry, and organic petrology were performed on the Carboniferous-Permian (C–P) coaly source rocks in the Huanghua Depression, Bohai Bay Basin. The oil-generated parent macerals of coal's secondary oil generation process (SOGP) were mainly hydrogen-rich collotelinite, collodetrinite, sporinite, and cutinite, while the oil-generated parent macerals of tertiary oil generation process (TOGP) were the remaining small amount of hydrogen-rich collotelinite, sporinite, and cutinite, as well as dispersed soluble organic matter and unexhausted residual hydrocarbons. Compared with coal, the oil-generated parent macerals of coaly shale SOGP were mostly sporinite and cutinite. And part of hydrogen-poor vitrinite, lacking hydrocarbon-rich macerals, and macerals of the TOGP, in addition to some remaining cutinite and a small amount of crude oil and bitumen from SOGP contributed to the oil yield. The results indicated that the changes in oil yield had a good junction between SOGP and TOGP, both coal and coaly shale had higher SOGP aborted oil yield than TOGP starting yield, and coaly shale TOGP peak oil yield was lower than SOGP peak oil yield. There were significant differences in saturated hydrocarbon and aromatic parameters in coal and coaly shale. Coal SOGP was characterized by a lower Ts/Tm and C_{31}-homohopane22S/(22S+22R) and a higher Pr/nC_{17} compared to coal TOGP, while the aromatic parameter methyl dibenzothiophene ratio (MDR) exhibited coaly shale TOGP was higher than coaly shale SOGP than coaly TOGP than coaly SOGP, and coal trimethylnaphthalene ratio (TNR) was lower than coaly shale TNR. Thus, we established oil generation processes and discriminative plates. In this way, we distinguished the differences between oil generation parent maceral, oil generation time, and oil production of coaly source rocks, and therefore, we provided important support for the evaluation, prediction, and exploration of oil resources from global ancient coaly source rocks.

1. Introduction

Carboniferous-Permian (C–P) coal-bearing strata deposited in several basins around the world have a high potential for petroleum

* Corresponding author.
E-mail address: chengfq9804@163.com (F.-Q. Cheng).

https://doi.org/10.1016/j.petsci.2023.11.011

generation, and the oil and gas reserves of these strata used for hydrocarbon supply account for 12.6% of all oil- and gas-bearing formations (Jiang et al., 2018; Wang et al., 2020). For example, the accumulated hydrocarbon expulsion amount of C–P coaly source rock in Ordos Basin is 2.38×10^{14} m^3, and oil and gas in Donets Basin of Ukraine mainly originate from C–P coaly source rock (petroleum equivalent is slightly bigger than 1.57×10^8 t) (Misch et al., 2015; Wang et al., 2016a). The C–P coaly source rocks also have abundant oil and gas potential in the Bohai Bay Basin. For instance, the total natural gas resources of the C–P coaly source rocks are about 1.284×10^{12} m^3 in Huanghua Depression (Liao et al., 2003). Furthermore, oil and gas originating from C–P coaly source rocks have been found in several tectonic zones, such as the Suqiao-Wen'an slope and Wuqing Depression of Jizhong Depression, Wangguantun buried hill, and Kongdian uplift of Huanghua Depression, which all belong to Bohai Bay Basin (Yu et al., 2018; Zhao et al., 2019). A relevant study indicates that the C–P (Taiyuan Shanxi Formation) coaly source rocks, which are deposited in the Bohai Bay Basin in a marine terrestrial transitional environment, consist of coal, coaly shale, carbonaceous shale, and dark shale (Collinson et al., 1994; Figueiredo et al., 2010; Zhao et al., 2018). The coal-bearing strata of the Taiyuan Formation were formed in the peat flat under the sedimentary system of land surface sea fortress island. These coal-bearing strata were influenced by frequent sea invasion and sea retreat, and by accumulated and preserved rich aquatic organisms under anoxic conditions (Li et al., 2016; Li et al., 2019). The coal-bearing stratigraphic deposits of the Shanxi Formation are characterized by a shallow water delta plain peat swamp coal accumulation environment, and the coaly shale accumulation occurs in the delta plain sediments of the Shanxi Formation, both of which exhibit regular spatial and temporal evolution (Lou et al., 2022; Wang et al., 2016). Controlled by sedimentary environment and organic matter supply, the oil-generated parent macerals of coaly source rocks are primarily vitrinite, including collodetrinite, collotelinite, and corpogelinite, followed by inertinite, with the least content of liptinite (Michelsen and Khorasani, 1990; Xu et al., 2021). For example, the content of vitrinite in Qikou sag coaly source rocks can reach 80%, and in Beidagang buried hill coaly source rocks, it is generally 20% (Gong et al., 2022). Hydrogen-rich collodetrinites and liptinite (e.g., cutinite, spirinite, and collodetrinite) are the main oil-generated parent macerals of coaly rocks (Li et al., 2008; Tewari, 2015). Coal has a higher oil generation potential because of the presence of cutinite and spirinite in hydrogen-rich collotelinite and liptinite. In contrast, coaly shale has a lower oil generation potential than coal due to the presence of less spirinite, cutinite, and vitrinite, and because it is being oxidized by terrigenous clastics (Qi et al., 2020; Xu et al., 2021). Meanwhile, with the influence of multiple uplifts and burial processes, the oil-generated parent material changes from insoluble kerogen and dispersed soluble organic matter to crude oil and asphalt (Xu et al., 2021), and residual kerogen and undeleted residual hydrocarbon are the main oil-generated parent macerals for multi-time oil generation processes (Zhao et al., 2011). The results of previous structural studies demonstrated that the C–P system strata in the Bohai Bay Basin experienced multiple tectonic subsidences and uplifts after sedimentation (Zhang et al., 2019). They chiefly experienced three burial-uplift alternating evolutions of Hercynian Indosinian, Yanshanian, and Himalayan periods (Yan et al., 2020), and consequently, the Mesozoic Yanshanian tectonic differentiation was intensified. Tectonism and sedimentary filling play an important role in controlling the thermal evolution of the basin (Jia et al., 2022; Guo et al., 2022). This complex burial process led to the occurrence of a multi-time oil generation process (i.e., a time-dependent oil generation process) (Zhang et al., 2019; Zhao et al., 2019). Since the Triassic, the C–P coaly source rocks in Huanghua Depression have experienced two or three important oil generation processes. The late Himalayan is considered the most significant oil generation and expulsion time for oil accumulation (Jin et al., 2009). Xu et al. (Xu et al., 2021; Xu and Jin, 2020a) found that the multi-phase hydrocarbon generation potential of C–P coaly rocks is closely related to the hydrocarbon generation times, hydrocarbon generation parent macerals, and lithology. They also reported that the hydrocarbon generation output decreased with the increase of the initial R_o of the secondary hydrocarbon generation process, and the hydrocarbon generation amount of coal was much higher than that of coaly shale. These studies predominantly focused on the geological conditions, hydrocarbon generation evolution, and hydrocarbon generation potential of C–P coaly source rocks, which clarified the characteristics of a multi-time oil generation process, and determined oil-generated parent macerals composition of coal-measure source rocks (Lou et al., 2022; Wang et al., 2022). However, there is a lack of research on the composition of initial oil-generated parent macerals in different oil generation processes and the junction of oil generation processes at different times, which is not conducive to an in-depth understanding of oil generation laws in different lithologies and times. Besides, there are important doubts about the potential of oil and gas production from different lithologies and times of C–P (Jin, 2023).

We studied the oil-generated parent macerals, the oil production potential of coaly source rocks in different lithologies, and oil generation times of C–P in Huanghua Depression by using high-temperature and high-pressure thermal simulation experiment, determination of total organic carbon content, rock pyrolysis, maceral identification, biomarker analysis, and other experiments. To distinguish the evolution process differences of oil-generated parent macerals and oil production at different times, to reveal the differences of oil and gas generation in different evolution stages, and to uncover the junction mechanism of SOGP and TOGP, we established oil and gas product identification charts of source rocks in different times and provided more valuable information for the subsequent evaluation and exploration of oil and gas potential of C–P coaly source rocks.

2. Geological setting

The Huanghua Depression is an important hydrocarbon-bearing area in the central part of the Bohai Bay Basin in eastern China (Qu et al., 2018). It is connected to the Cangxian Uplift by the Cangdong Fault to the west, is adjacent to the Yanshan fold belt by the Beitang and Nanbu depressions to the north, has undergone an overlying or faulted transition to the Haizhong-Chengning Uplift to the southeast, and is an asymmetric narrow fracture basin converging in the SW direction and spreading out in the NE direction, with a total area of about 1.7×10^4 km^2 (Fig. 1a (Li et al., 2019)). The C–P strata are principally composed of Benxi Formation, Taiyuan Formation, Shanxi Formation, and Shihezi Formation (Fig. 1c (Hou et al., 2017)), among which the coaly source rocks are deposited in Taiyuan and Shanxi Formations. The C–P strata can be 600–1100 m thick and shows greater thickness in the southern region compared to the northern region. The coal seams in C_2t are relatively thick, averaging 20–25 m, and P_1s is generally of 10–15 m (Zhao et al., 2018). Taiyuan Formation is mainly composed of peat flat and lagoon sediments, containing thin layers of sandstone, limestone, and coaly source rock, and a thick layer of black shale, which belongs to marine-terrestrial interaction sedimentation. The Shanxi Formation is characterized by coastal marsh sediments in the delta front, where carbonaceous shale, sandstone, thin coal, and delta facies dark coaly shale are developed (Gong et al., 2022). The sedimentary environment dominated by marine continental transitional facies

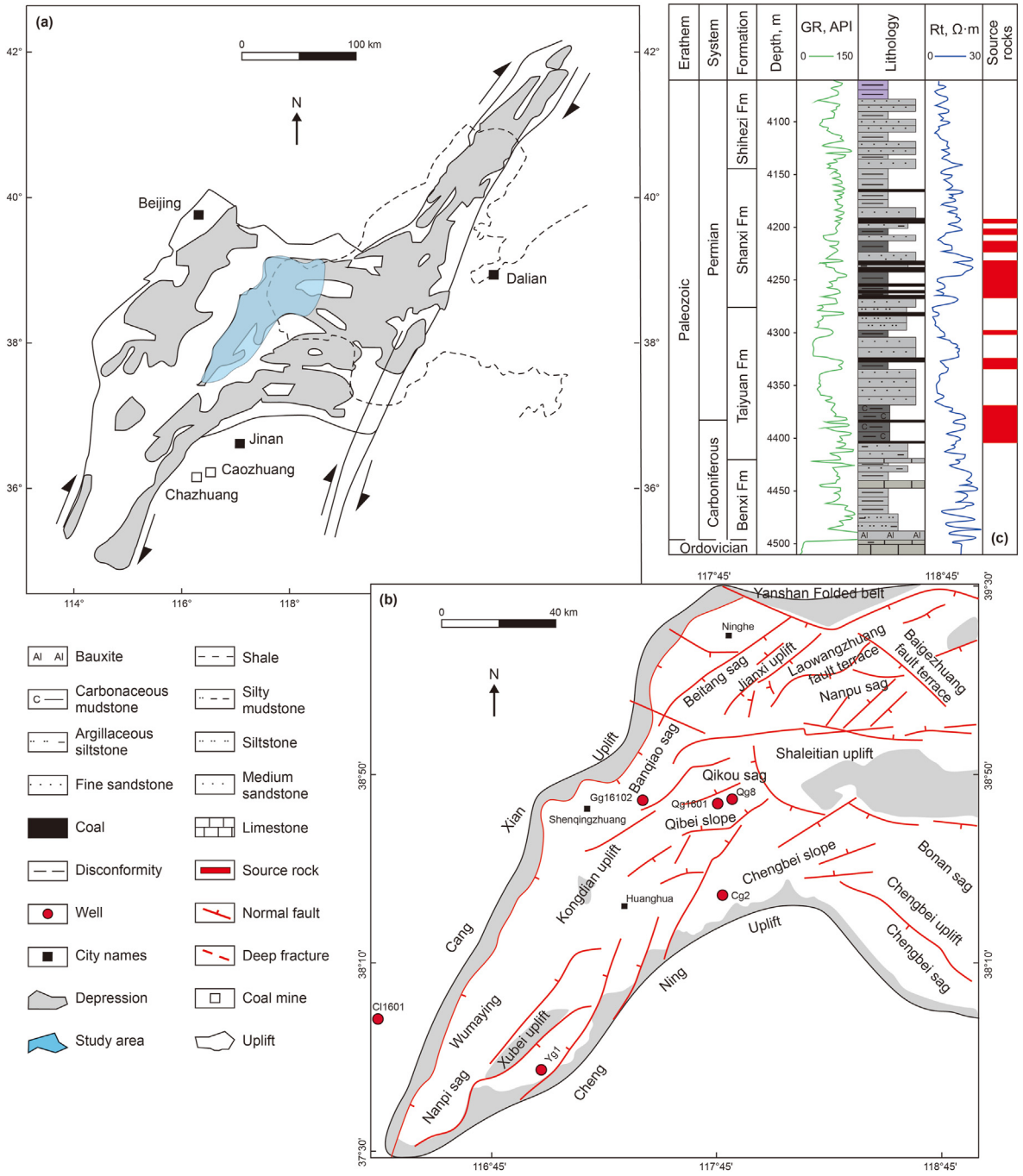

Fig. 1. Structural map and geographic profile of the Carboniferous-Permian coaly source rocks in the Bohai Bay Basin (modified from Xu and Jin, 2020b). **(a)** Bohai Basin; **(b)** research area; **(c)** stratigraphic sequence.

has increased the complexity of oil-generated parent macerals of coaly source rocks with different lithologies, which has resulted in the diversification of oil and gas production (from crude oil, light oil, condensate to kerogen-cracking gas, oil-cracking gas, and asphalt-cracking gas) (Guan et al., 2010; Schenk et al., 1997). At the same time, Huanghua Depression was affected by the superposition of multiple tectonic movements, and the burial history of the Upper Paleozoic mostly experienced the alternating evolution of three burial-uplift cycles of Indosinian, Yanshanian, and Himalayan periods (Bo et al., 2022). Hercynian-Indosinian regional subsidence promoted the primary hydrocarbon generation of C—P coaly source rocks in the early and middle Triassic (Xu and Jin, 2020a). Differential tectonic uplift and subsidence occurred in the Yanshanian period, and most areas from Jurassic (J) to Cretaceous (K) underwent uplift or continuous subsidence, and SOGP occurred in coaly source rock (Zhang et al., 2019). The tectonic superimposition during the Himalayan period prompted SOGP and TOGP to bury deep in the shallowly buried area again or in the deeply buried area continuously in the late Cretaceous (Xu and Jin, 2020a). The tectonic evolution history of the study area is very complex, with several sedimentary discontinuities and uplift denudations, which has led to regional structural differences (Zhao et al., 2018), and

thus, different geothermal evolution stages and substantial hydrocarbon generation diversity in Huanghua Depression (Zhao et al., 2019). The measured data of many drilling samples in the early stage indicate that the total organic carbon (TOC) content of coal varies from 20.5% to 75.0%, with an average of 45.6%, S_1+S_2 is in the range of 60.0–300.0 mg/g, and the TOC content of coaly shale varies from 0.2% to 14.8%, with an average of 4.32%, S_1+S_2 is in the range of 0.4–20.1 mg/g. The overall organic matter abundance of coaly shale to coal is from poor to good (He et al., 2016; Zhao et al., 2019). Most coaly source rocks buried above 3500 m have vitrinite reflectance values of lower than 0.70%. With an increasing burial depth, the degree of thermal evolution in the source rocks varies from 0.76% to 1.50%, indicative of secondary thermal evolution. The source rocks buried beneath 3500 m reached the oil window and wet gas stage (Li et al., 2016; Chang et al., 2018).

3. Samples and methods

3.1. Samples

A total of 98 samples were selected from the C–P coaly source rock cores of wells GG16102, CG2, CL1601, DT1, KG4, QG8, WS1, YG1, YG2, QG11X1, and QG1602 in Huanghua Depression, including 31 coal samples, 24 carbonaceous mudstone samples, and 38 coaly shale samples. Two representative samples of coal and coaly shale from wells GG16102 and CG2 were selected to conduct the thermal simulation experiment. The organic geochemical analysis, including rock pyrolysis analysis, determination of TOC content, vitrinite reflectance, and kerogen maceral determination, was performed on the above samples, as well as the heated sample residues, and the produced oil and gas (Figs. 2, 3 and 6).

3.2. Analytical methods

3.2.1. Thermal simulation experiments

The Upper Paleozoic strata in Huanghua Depression have experienced three alternating burial uplift evolution. The experimental design was based on the second part of the article and the hydrocarbon generation and evolution history established by predecessors (Xu and Jin, 2020b). In this experiment, a thermal simulation experimental apparatus capable to withstand high temperatures and high pressures of up to 800 °C and 120 MPa in a closed system was selected. First, we loaded about 5 g of 80 mesh powder sample with 2.5 mL of distilled water into the autoclave, and then the sealed autoclave was evacuated and filled with 0.1 MPa nitrogen gas. After closing the valve of the autoclave, the temperature was first increased to 250 °C and then increased from 335 to 400 °C at different rates for a total of ten temperature points (two samples were naturally cooled down from 400 to 390 °C and to 380 °C, respectively). Another experiment was conducted with the same heating rate up to 400 °C and then the temperature was reduced to 250 °C, and after that, it was raised to 380–510 °C with a total of eight points. We have counted the maturity from 335 to 510 °C with a total of 12 temperature points (Fig. 2). Finally, dichloromethane was utilized to repeatedly extract the residue samples, and the collected produced liquid and residues were measured and analyzed.

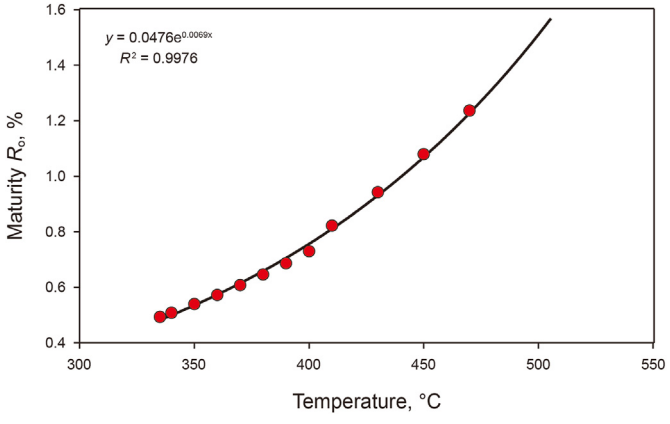

Fig. 2. Relationship between simulated temperature and maturity of coal and coaly shale.

3.2.2. Total organic carbon and Rock-Eval pyrolysis

The TOC content of the sample powder (~200 mesh) was measured with a LECO CS–230 analyzer. The carbonates were removed with dilute HCl at 60 °C, and then we analyzed about 200 mg of each powder sample after washing the sample with distilled water to remove HCl and drying at 50 °C for 24 h. The TOC values were measured based on the Chinese National Standard GB/T 19143-2017 (Li et al., 2008).

The samples were analyzed by Rock-Eval 7. Each crushed sample (~100 mg) was heated in a helium atmosphere at a programmed rate of 50 °C/min from 300 to 550 °C to obtain S_1, S_2, S_3, and Tmax. Rock pyrolysis test conformed to GB/T 18602-2012 (Li et al., 2008).

3.2.3. Organic petrology analysis

All samples were analyzed for vitrinite reflectance (R_o) using a Leica DM4500P microscope according to the protocol of International Standard (ISO 17246:2010) and Chinese Petroleum Industry Standard (SY/T 51242012). Sapphire (R_o = 0.59%) and gadolinium gallium garnet (R_o = 1.73%) were used as standard samples. A total of 13 polished samples were selected for petrographic analysis, and all microfraction compositions as well as their volume percentages were measured from the total microfraction (Liu et al., 2020).

3.2.4. Gas chromatography-mass spectrometry (GC–MS) analysis

For GC-MS analysis, the thermal simulation residue and other samples were crushed and extracted separately in a Soxhlet extractor (solvent was dichloromethane) for 72 h. The resulting oil samples were soaked in hexane for 24 h to remove asphaltenes. Saturated hydrocarbons, aromatics, and nitrogen and sulfur oxides compounds (NSO) were separated from each sample to perform the analysis by using silica-alumina column chromatography. These analyses were conducted using an Agilent 7890 gas chromatograph with an HP-5MS fused silica column and helium as the carrier gas linked to 5975C mass spectrometers. The data after analysis was interpreted using Agilent MsaaHunter Workstation software. The chromatographic ramp-up procedure for saturated and aromatic hydrocarbons was as follows: start at 35 °C, constant temperature for 10 min, then 0.5 °C/min to 60 °C, then 2 °C/min to 200 °C, finally 4 °C/min to 280 °C, constant temperature for 5 min, and a split ratio of 10:1 (Li et al., 2015).

4. Results

4.1. Bulk organic geochemical characteristics of source rocks

The results of sample measurement showed that the TOC content of coal samples was higher than that of coaly shale, and the distribution was more concentrated. Coal had higher S_1 and S_2 than coaly shale, and the distribution range of Tmax was the same (Fig. 3). TOC of the coal and coaly shale ranged from 60.70% to 75.8% and from 3.58% to 4.35%, respectively, and the coal hydrocarbon generation potential (S_1+S_2) ranged from 14.23 to 143.46 mg/g,

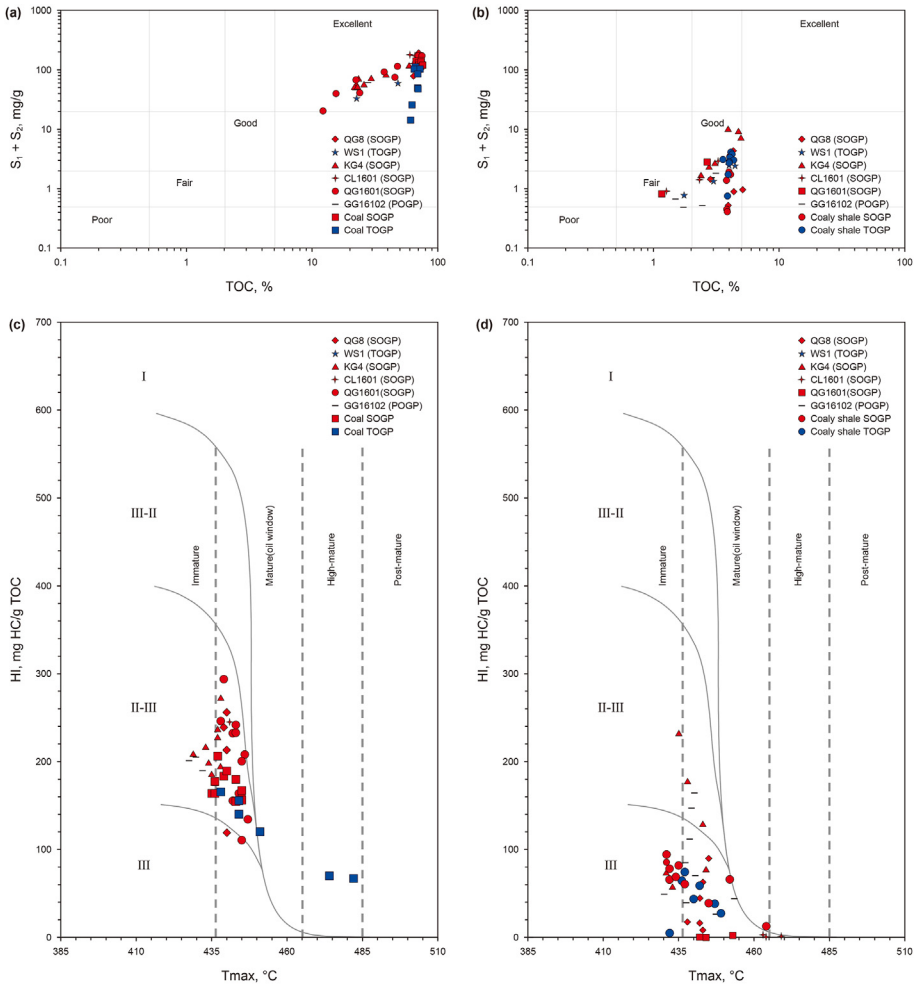

Fig. 3. Organic matter abundance of coaly source rocks. POGP: Primary oil generation process; SOGP: Secondary oil generation process; TOGP: Tertiary oil generation process.

which was in the excellent quality range, while the coaly shale only reached fair to good quality. The S_1+S_2 of both coal and coaly shale from SOGP wells was larger than that of the samples from TOGP wells, but the demarcation in TOC was not distinct (Fig. 3a and b). The intersection plots of Rock-Eval Tmax and hydrogen index (HI) exhibited significant variability in kerogen types. The coal samples displayed a higher HI, which was about twice as high as that of the coal mudstone, and almost all samples were in the type II-III area, and the coaly shale was chiefly distributed in the type III area, while a few reached type II-III. The coal samples showed a higher HI (21.29–293.86 mg/g TOC, mean 180.68 mg/g TOC), which was about twice as high as that of the coaly shale, and almost all samples were in the type II-III area, and the coaly shale was primarily distributed in the type III area, while a few reached type II-III. HI of both coal and coaly shale exhibited a decreasing trend in the process of SOGP to TOGP (Fig. 3c and d).

4.2. SOGP and TOGP of coal and coaly shale

The SOGP and TOGP of coal and coaly shale displayed different evolutionary patterns. When the temperature reached 340 °C (R_o = 0.49%), coal entered the SOGP, and the coal oil yield increased for the first time continuously, and then the yield showed a small decrease under the decreasing temperature, and the oil yield reached the maximum value of 96.05 mg/g TOC at the temperature of 400 °C (R_o = 0.73%). The SOGP had a similar trend and good junction with the TOGP, but the yield decreased rapidly after reaching the peak of oil production. The oil yield at the TOGP oil peak (R_o = 0.91%) was 101.09 mg/g TOC, which was slightly higher than the SOGP oil peak, however, at the initial maturity point (380 °C, R_o = 0.83%), the oil yield was 80.49 mg/g TOC, which was much different from the initial SOGP yield (Fig. 4a). Compared with coal, the oil yield of coaly shale was significantly different. In the coaly shale SOGP, the oil yield increased rapidly with temperature and reached the oil peak (R_o = 0.77%) with a yield of 89.45 mg/g TOC. The TOGP yield was 79.93 mg/g TOC at a heating temperature of 410 °C (R_o = 0.90%). The oil peak TOG of coaly shale was also lower than SOGP, and both were lower than that of coal. Both coal and coaly shale had a higher SOGP aborted oil yield compared to TOGP starting yield. However, the yield (26.03 mg/g TOC) of coaly shale TOGP at final heating (510 °C) was about three times that of coal (Fig. 4b).

4.3. Variation of organic petrographic characteristics

The composition of the oil generation parent maceral and the content of coal and coaly shale was obviously diverse. The vitrinite in coal was the main maceral component (81.4%–89.8%), which contained a large amount of hydrogen-rich collodetrinite, collotelinite, and corpogelinite. Lipinite + huminite content accounted for 0.6%–7.7% of coal, while it accounted for 0.3%–3.0% of coaly shale. The vitrinite of coal rock was composed of telinite, collotelinite, and

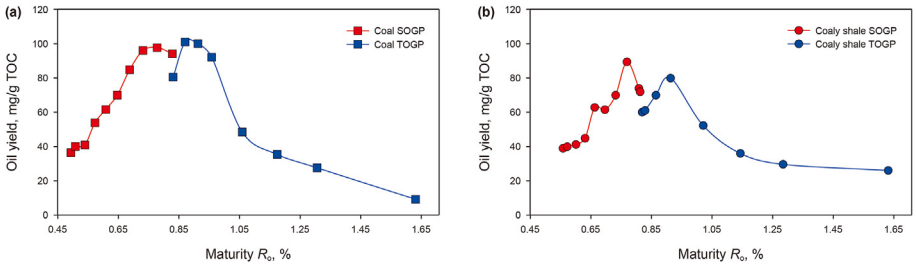

Fig. 4. Oil yield of coal and coaly shale during SOGP and TOGP.

corpogelinite (Fig. 5b$_2$, 5b$_3$ and 5b$_4$). The liptinite component included hydrogen-rich and oil-generation components such as cutinite, sporinite, and telaginite, showing brown yellow, yellow, and other fluorescence characteristics (Fig. 5a$_1$ and 5b$_1$), and inertinite consisted of fusiniteand and semifusinite (Fig. 5a$_2$ and 5b$_3$). Bright yellow-white strawberry-like pyrite was widespread in the coaly shale with a certain amount of gray-black clay mineral matrix (Fig. 5c$_3$), accompanied by small amounts of cutinite and sporinite (Fig. 5a$_4$). Furthermore, a few telalginites filled in the particle space were also observed in the coaly shale sample (Fig. 5c$_1$).

The relative contents of different oil generation parent maceral compositions of coaly source rocks changed abruptly during SOGP and TOGP. The Hydrocarbon-rich vitrinite content of the coal sample was higher and rapidly decreased from 15.8% to 10.5% to 0, respectively, during SOGP and TOGP. While the coaly shale vitrinite content was extremely low and changed little with thermal evolution, it was not the main contributing component of organic matter hydrocarbon generation of coal rock (Fig. 6a). The main oil-generated parent macerals were cutinite and sporinite in the liptinite. Sporinite was more than cutinite in coal, and the

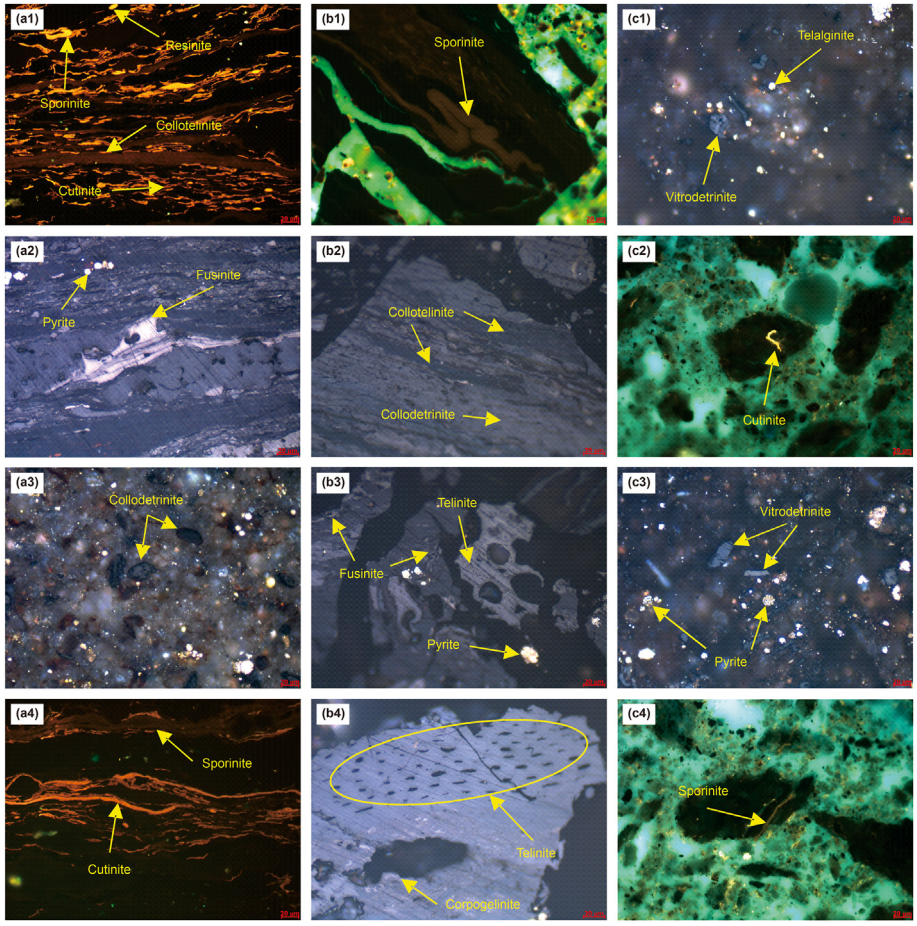

Fig. 5. Maceral components in coaly source rocks. **(a$_1$)** sporinite, cutinite, collotelinite, resinite, coal, unheated, Taiyuan Formation, 500 × , excited by blue light; **(b$_1$)** sporinite, coal, 340 °C, Taiyuan Formation, 500 × , excited by blue light; **(c$_1$)** telalginite, vitrodetrinite, coaly shale, 335 °C, Shanxi Formation, 500 × , oil-immersed reflective light; **(a$_2$)** pyrite, fusinite, coal, unheated, Taiyuan Formation, 500 × , oil-immersed reflective light; **(b$_2$)** collodetrinite, collotelinite, coal, 350 °C, Taiyuan Formation, 500 × , oil-immersed reflective light; **(c$_2$)** cutinite, coaly shale, 370 °C, Shanxi Formation, 500 × , excited by blue light; **(a$_3$)** collodetrinite, coaly shale, unheated, Shanxi Formation, 500 × , oil-immersed reflective light; **(b$_3$)** telinite, fusinite, pyrite, coal, 370 °C, Taiyuan Formation, 500 × , oil-immersed reflective light; **(c$_3$)** vitrodetrinite, pyrite, coaly shale, 400-250-430 °C, oil-immersed reflective light; **(a$_4$)** sporinite, cutinite, coaly shale, unheated, Shanxi Formation, 500 × , excited by blue light; **(b$_4$)** telinite, the cavity is filled with clay minerals, corpogelinite, coal, 400-250-510 °C, Taiyuan Formation, 500 × , oil-immersed reflective light; **(c$_4$)** sporinite, coaly shale, 400-250-470 °C, Shanxi Formation, 500 × , excited by blue light.

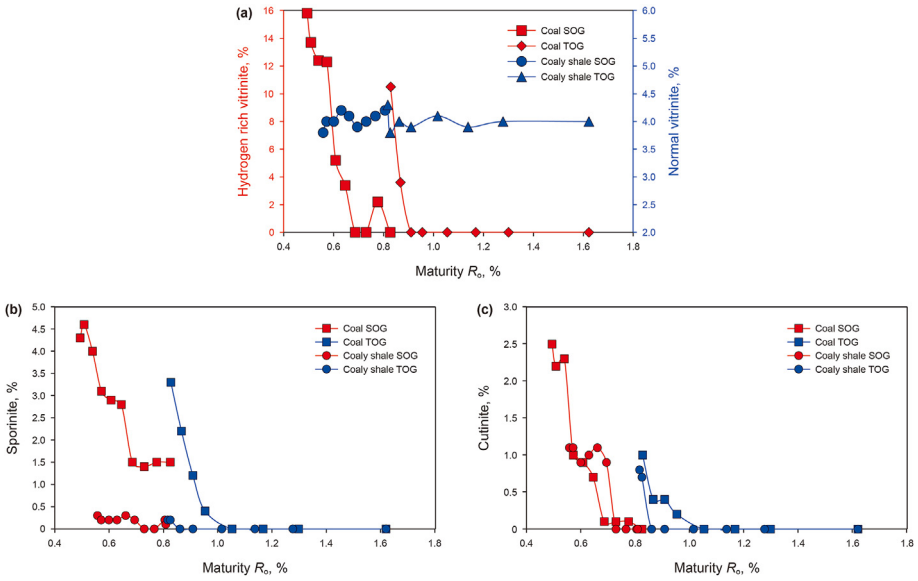

Fig. 6. Relationship between parent macerals and maturity of coal and coaly shale.

consumption in each oil generation time was also greater than cutinite. On the contrary, the content of the sporinite was less than that of the cuticle, and the content of both diminished from 0.3% to 1.1% to 0, respectively (Fig. 6b and c). In both SOGP and TOGP, the content of cutinite and sporinite in the liptinite was much higher in coal than in coaly shale, which was almost depleted after Ro reached 1.05%. And coaly shale exhibited a trend of increasing content of hydrogen-poor secondary fraction with increasing maturity at high maturity time (Fig. 6).

4.4. Evolutional characteristics of saturated hydrocarbon- and aromatic hydrocarbon-related parameters derived from coaly source rock

The analysis of the test results of biomarker compounds revealed that there were evolutionary differences between the production of coal and coaly shale during the thermal simulation of SOGP and TOGP in terms of the series of compounds such as *n*-alkanes, isoalkanes, hopane, fluorene, and naphthalene (Fig. 7). Coal $\Sigma C_{21-}/\Sigma C_{22+}$ was smaller than that of coaly shale, but both displayed an increasing trend with the increase of thermal evolution. The ratio of $\Sigma C_{21-}/\Sigma C_{22+}$ in coal SOGP (0.51–1.69) and coaly shale SOGP (1.38–3.24) fluctuated greatly and presented a stable upward trend during the coal TOGP (0.83–1.80) at the high maturity stage (Fig. 8a). Pr/nC_{17} showed strong discrimination ability, and Pr/nC_{17} of coal (0.15–0.64) was lower than that of coaly shale (0.27–0.76), and SOGP of coal and coaly shale was higher than the corresponding TOGP of coal and coaly shale. Compared to coal, coaly shale had a better junction from SOGP to TOGP. And at the junction point of two hydrocarbon generation in coal, the Pr/nC_{17} of TOGP was slightly higher than that of SOGP (Fig. 8b). There were also obvious evolutionary differences between SOGP and TOGP of hopane series compounds. Ts/Tm was unchanged and almost stable in the SOGP of coal and coaly shale with small fluctuations, but there was a substantial upward trend in the TOGP process (Fig. 8c). Coal SOGP and TOGP exhibited higher (> 0.56) and more stable C_{31}22S/(22S+22R) values, while coaly shale showed lower C_{31}22S/(22S+22R) values (0.51–0.60), and the ratio of TOGP was slightly higher than SOGP. Whether coal or coaly shale, Ts/Tm and C_{31}22S/(22S+22R) exhibited a smooth transition at the junction of the two hydrocarbon generation processes (Fig. 8d). Aromatic biomarker compound parameters, such as TNR and MDR, both displayed similar smoothly increasing trends with thermal evolution, and the MDR parameters of coaly and coaly shale were clearly distinguished, with a clear MDR demarcation between coaly shale (0.76–1.15) and coal (0.53–0.70) during SOGP (Fig. 8e and f).

5. Discussion

5.1. Evolutional differences on parent maceral in multi-time oil generation processes of coaly source rock

The organic matter abundance and the type and content of oil-generated parent macerals in C–P coal and coaly shale of Huanghua Depression exhibited significant differences with the degree of thermal evolution, and their changing trends were also different during the SOGP and TOGP (Rangel et al., 2002; Tewari and Khan, 2015; Xu et al., 2021). Differences in the composition and content of the oil-generated parent macerals of coal and coaly shale led to differences in their hydrocarbon generation potential during different times of oil generation (Xu and Jin, 2020b). Coal is deposited in an acidic and moist swampy environment, thus, the stable environment allows it to accumulate more hydrogen-rich collotelinite and collodetrinite, and hydrogen-rich sporinite and cutinite are derived from terrigenous woody and herbaceous plants (Li et al., 2019; Van Krevelen, 1993). These hydrogen-rich macerals are cemented together through biodegradation, gelation, and input of various terrigenous detritus. In contrast, the coaly shale formed in a shallow deltaic environment of the Taiyuan Formation has insufficient hydrogen-rich components, and instead, mostly hydrogen-poor vitrinite and a small amount of bituminous organic matter and exinite are accumulated in it (Li et al., 2019; Xu et al., 2021). The difference in depositional environments causes the coal to have more hydrogen-rich macerals than coaly shale (e.g., hydrogen-rich collodetrinite, sporinite, and cutinite of liptinite), contributing to the considerably higher organic matter abundance and hydrocarbon generation potential of coal than coaly shale (Figs. 3a, 3b, 5, 6 (Petersen et al., 2000; Tewari and Khan, 2015)). The S_1+S_2 value of coal ranged from 14.23 mg/g to 143.46 mg/g, which was of excellent quality. In contrast, the S_1+S_2 of coaly shale

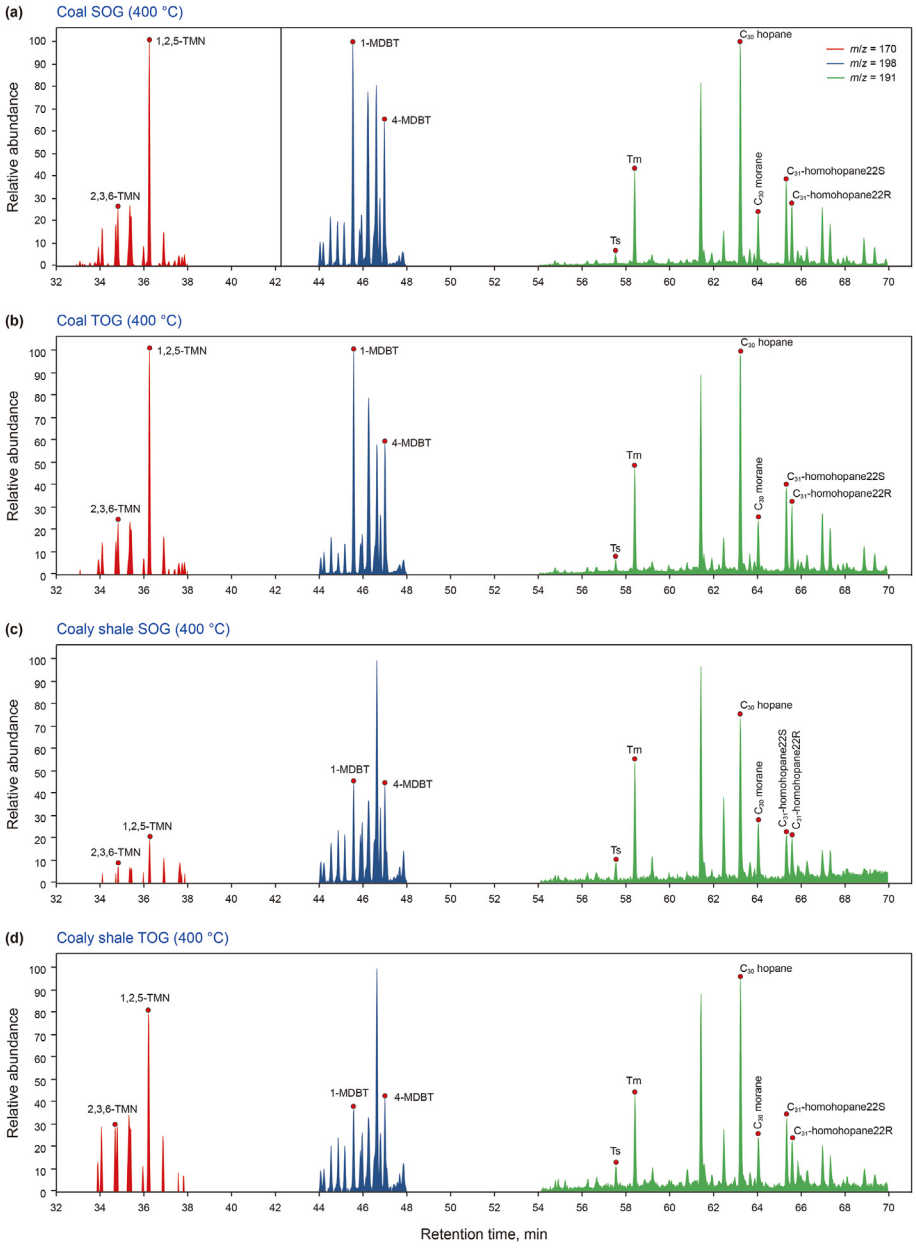

Fig. 7. Chromatography of hopane series (m/z = 191), fluorene series (m/z = 198), and naphthalene series (m/z = 170) compounds. Ts:18α(H)-22,29,30-C_{27}hopane; Tm:17α(H)-22,29,30-C_{27}hopane; 1,2,5-TMN: 1,2,5-Trimethylnaphthalene; 2,3,6-TMN:2,3,6-Trimethylnap-hthalene; 1-MDBT:1-Methyldibenzothiophene; 4-MDBT:4-Methyl dibenzothiophene.

was much lower than that of coal, with an average value of only 2.43 mg/g, and the average value of coal TOC (69.60%) was also much higher than the average value of coaly shale TOC (4.01%) (Fig. 3a and b). The consumption of oil-generated parent macerals during SOGP and TOGP in coaly source rocks indicated that hydrogen-rich vitrinite and liptinite (especially collodetrinite, sporinite, and cutinite) were the main oil generation components for coal, while inertinite and huminite contributed to oil generation very weakly (Fig. 6 (Chen et al., 2017; Li et al., 2008)). The main hydrocarbon generation components of SOGP and TOGP were the same, and the very low content of resinite in the early time of SOGP promoted the formation of oil slightly (Fig. 5a_1), and the oil-generated parent macerals during peak oil generation were dominated by sporinite, cutinite, and hydrogen-rich collotelinite (Fig. 6). Although the previous two oil generation processes consumed a large amount of oil-generated parent macerals, the remaining hydrogen-rich components and the residual hydrocarbon from SOGP still caused a high peak of TOGP oil yield (Fig. 4). Liptinite (especially cutinite) was the main oil-generated parent macerals of coaly shale, and vitrinite had no hydrocarbon donor capacity during the evolution of coaly shale SOGP and TOGP. During coaly shale SOGP, the oil-generated parent macerals also contained residual sporinite and cutinite, dispersed soluble organic matter, undischarged residual hydrocarbons, and solid bitumen from the POGP (Zhao et al., 2011; Zheng et al., 2009). Except for part of the remaining cutinite, a small amount of crude oil and bitumen from SOGP contributed to its oil yield in TOGP (Fig. 5 (Xin et al., 2010)), and a few hydrogen-poor secondary components were also generated in the coaly shale (Fig. 6).

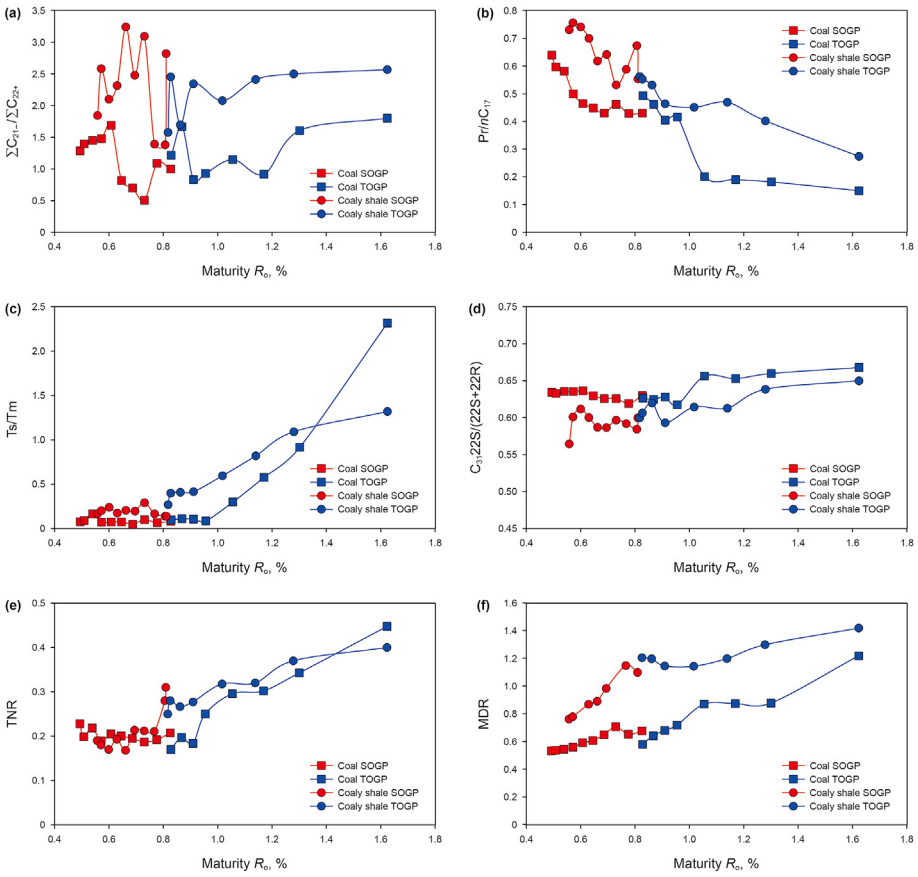

Fig. 8. Variations in parameters of saturated hydrocarbon and aromatic hydrocarbon in the thermal simulation. Pr: pristane; Ph: phytane; TNR = 2,3,6-TMN/(2,3,6-TMN+1,2,5-TMN); MDR = 4-MDBT/1-MDBT; C_{31}S/(S+R): C_{31}-homohopane22S/(22S+22R).

5.2. Junction law of multi-time oil generation of coaly source rock

C–P coal and coaly shale differ in terms of the chemical structure of oil-generated parent macerals due to different depositional environments, and the oil-generated parent macerals and yield of SOGP and TOGP and their transitional overlap also change regularly with the increase of stratigraphic depth (Xu et al., 2021; Xu and Jin, 2020b; Zhao et al., 2019). At the end of coal SOGP, the oil generation process was not completely stopped (Chang et al., 2018; Xu and Jin, 2020b), and the change in maceral content and oil yield suggested that the original residual hydrogen-rich vitrinite and lipinite were still generating oil with low yield, while the coaly shale did not have adequate hydrogen-rich vitrinite and other oil supply compositions (Fig. 6), resulting in a slightly lower oil yield at the end of the SOGP (Fig. 4b). Due to local deep burial in the Himalayan period, and shallow uplift and continuous deep burial followed by deep burial in the Late Cretaceous, SOGP stopped when the paleotemperature exceeded the corresponding maximum temperature, and TOGP occurred before SOGP stopping and had a good junction (Xu and Jin, 2020b; Zhu et al., 2010; Jia et al., 2021). At this time, the initial R_o of coal and coaly shale TOGP was 0.82% and 0.81%, respectively, and the oil-generated parent macerals of coal were transformed from residual hydrogen-rich collotelinite, collodetrinite, spirinite, cutinite, and pre-oil bitumen to a small amount of cutinite and secondary organic matter (heavy oil, post-oil bitumen, and pyrobitumen) (Liu et al., 2020; Schenk et al., 1997). The rise in temperature leads to the cracking of oil and gas and solid residues (solid bitumen and pyrobitumen), and consequently, the heavy oil is converted into light hydrocarbons and residual insoluble bitumen (Liu et al., 2020; Mastalerz et al., 2018). Meanwhile, the biodegradation of oil by microorganisms and the de-asphalting of oil cause the initial oil yield of coal TOGP to be supplemented (Fig. 6 (Misch et al., 2019)). Oil-generated parent macerals of coaly shale SOGP were largely sporinite and cutinite, which were rapidly consumed at the junction of SOGP and TOGP. After the temperature exceeded 400 °C, sporinite, cutinite, resinite, and telaginite stopped generating oil or slightly generated oil (Chen et al., 2017; Lee and Sun, 2016). The less oil-generated parent macerals in TOGP not only resulted in the decline of oil yield but also caused the peak of oil to reach at a higher temperature. Affected by the rapid burial depth of the strata, there was a higher oil generation rate at the beginning of TOGP at the junction (Xu and Jin, 2020b). According to previous studies, the oil production potential begins to decrease as the starting R_o increases (Xu and Jin, 2020b; Zheng et al., 2009). The oil yield of coaly source rock SOGP and TOGP (Fig. 4), oil-generated parent macerals such as cutinite and sporinite (Fig. 6), and other biomarker parameters (Ts/Tm, C_{31}S/(S+R), Pr/nC_{17}, TNR, MDR) were close at the transition (Fig. 8), indicating that the two oil generation processes were well junctioned.

5.3. Differences and source identification of oil production from coaly source rock during multi-time oil generation processes

Affected by oil-generated parent macerals at different times, the compositions of coal and coaly shale oil production are different (Wang et al., 2018). The different biomarker compound ratios were used in oil production to differentiate the oil evolution processes in the coal and coaly shale at different times. The difference between

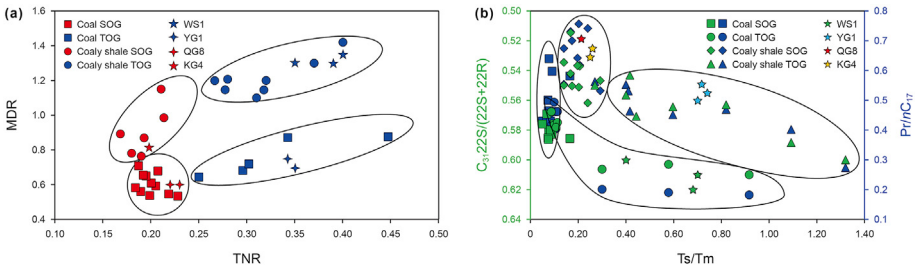

Fig. 9. Parameters of saturated hydrocarbon series compounds and MDR *vs.* TNR for distinguishing lithologies and times coming from thermal simulation.

the two oil generation processes of coal and coaly shale was observed during the thermal simulation using the good isoprenoid alkenes and hopane indicators such as Ts/Tm, $C_{31}S/(S+R)$, and Pr/nC_{17} (Fig. 9b). Coal SOGP was characterized by extremely low Ts/Tm (< 0.1) and a wide range of Pr/nC_{17} values. In addition to a wide range of Ts/Tm, the coal TOGP process was characterized by high $C_{31}S/(S+R)$ values. Compared with coal, coaly shale was more distinct. Coaly shale SOGP had a low $C_{31}S/(S+R)$ value and a high Pr/nC_{17} value, while TOGP Ts/Tm spaned a wider range (0.4–1.4) with $C_{31}S/(S+R)$ and Pr/nC_{17} both in the middle ratio. After putting the biomarker compound parameters of the saturated hydrocarbon of YG1, KG4, and WS1 wells into the plate, we found that coaly shale and coal belonged to SOGP and TOGP, respectively, which was consistent with the actual situation (Fig. 9b). Therefore, different times of coal and coaly shale were distinguished by Ts/Tm, $C_{31}S/(S+R)$, Pr/nC_{17}, and other saturated hydrocarbon indicators.

The parameters related to the maturity of aromatic compounds, mostly including TNR and MDR (Li et al., 2015; Radke et al., 1982; Radke et al., 1986), were used and fitted to the plates (Fig. 9). Combining the results of the above thermal simulation experiments and the established plates, we found that the SOGP and TOGP of coal and coaly shale were less different in terms of phenanthrene parameters, but were well distinguished by TNR and MDR. Coal SOGP was characterized by low TNR and low MDR, while its TOGP had high TNR, and MDR covered a wider range than SOGP. The MDR generally displayed a descending order of coaly shale TOGP is higher than coaly shale SOGP than coal TOGP than coal SOGP. Compared with coal, coaly shale SOGP was characterized by higher MDR and TNR values similar to coal SOGP, and the TNR and MDR values of coaly shale TOGP were the highest among the four. The coal had a lower TNR value than the coaly shale, while the TOGP of both lithologies had a higher MDR value than the SOGP (Fig. 9a). The coaly source rocks parameters of some C–P wells in Huanghua Depression also conformed to this classification.

The coaly source rocks of C–P in the Huanghua Depression have contributed to commercial-scale produced hydrocarbons, among which crude oil production is easier to identify and quantify, but the identification of oil production of different lithologies at different times is not yet clearly known. In our study, the two oil generation processes, SOGP and TOGP, in C–P coal and coaly shale were identified by biomarker compounds such as Ts/Tm, $C_{31}S/(S+R)$, Pr/nC_{17}, TNR, and MDR. This was consistent with the research results of Li et al. (Li et al., 2014; Meng et al., 2021). The biomarker compound parameters of wells WS1, YG1, QG8, and KG4 in the Huanghua Depression with different lithologies and different times were also consistent with this classification (Fig. 9). This plate provided a reference for global oil phase discrimination of similar C–P coaly source rocks (Fig. 9).

6. Conclusion

There were obvious differences in oil-generated parent macerals between C–P coaly source rocks in Huanghua Depression and multi-time oil generation processes. The oil-generated parent macerals of coal SOGP were primarily hydrogen-rich collotelinite and collodetrinite, and hydrogen-rich sporinite and cutinite, and the oil-generated parent macerals of TOGP were not only a small amount of hydrogen-rich collotelinite, sporinite, and cutinite left from SOGP but also dispersed soluble organic matter, unexhausted stagnant hydrocarbon, and solid bitumen. Compared with coal, oil-generated parent macerals of coaly shale SOGP lacked a large amount of hydrogen-high vitrinite, largely sporinite and cutinite. Besides, in addition to some of the remaining cutinite, there was a small amount of crude oil from SOGP and bitumen that contributed to its yield in TOGP. The difference in the type and content of oil-generated parent macerals caused the coal to have excellent quality with higher hydrocarbon generation potential in comparison to the coaly shale.

Compared with coaly shale, the coal had more hydrogen-rich macerals (e.g., hydrogen-rich collodetrinite, sporinite, and cutinite of liptinite), so coal was characterized by a higher oil yield peak and earlier SOGP. The oil yield of coal was also higher at the junction. But the TOGP yield of coal diminished faster, likely due to the lack of late oil-generated parent macerals. At the beginning of coaly shale TOGP, SOGP was still generating oil with low yield because of the existence of residual sporinite and cutinite, dispersed soluble organic matter, undischarged residual hydrocarbons, which promoted a good junction between the two oil generation processes. Both coal and coaly shale possessed higher SOGP aborted oil yield than TOGP starting yield.

The SOGP and TOGP of coal and coaly shale were clearly distinguished by biomarkers of saturated and aromatic hydrocarbons (such as Ts/Tm, $C_{31}S/(S+R)$, Pr/nC_{17}, TNR, and MDR). Through comparison with previous research results and data input of actual wells, we found that these plots provided theoretical support for the classification of oil generation times of C–P coaly source rocks in the Huanghua Depression and other oil and gas resources in areas with the similar geological background. For the sake of validation, more underground actual crude oil data are required to be compared with simulation results. Isotope can also be used to assist in subsequent research.

Declaration of competing interest

The authors declare that they have no known competing financial interests or personal relationships that could have appeared to influence the work reported in this paper.

Acknowledgement

The work presented in this paper was supported by the Certificate of National Science and Technology Major Project of the Ministry of Science and Technology of China (No. 2016ZX05006-007-004), the National Natural Science Foundation of China (Nos. 42172145, 42072130). We also thanks for the data support from PetroChina Dagang Oilfield Company.

References

Bo, S.S., Zhang, J.N., Han, G.M., Liang, C., Guo, Z.Q., 2022. Differential evolution of south and north structure in Huanghua depression. Bull. Sci. Technol. 38 (1), 20–25. https://doi.org/10.13774/j.cnki.kjtb.2022.01.004 (in Chinese).

Chang, J., Qiu, N.S., Zhao, X.Z., Shen, F.Y., Liu, N., Xu, W., 2018. Mesozoic and Cenozoic tectono-thermal reconstruction of the western Bohai Bay Basin (East China) with implications for hydrocarbon generation and migration. J. Asian Earth Sci. 160, 380–395. https://doi.org/10.1016/j.jseaes.2017.09.008.

Chen, J.P., Deng, C.P., Wang, H.T., Sun, X.G., 2017. Main oil generating macerals for coal-derived oil: a case study from the Jurassic coal-bearing Turpan Basin, NW China. Org. Geochem. 111, 113–125. https://doi.org/10.1016/j.orggeochem.2017.05.004.

Collinson, M.E., Van Bergen, P.F., Scott, A.C., De Leeuw, J.W., 1994. The oil-generating potential of plants from coal and coal-bearing strata through time: a review with new evidence from Carboniferous plants. Geol. Soc. Spec. Publ. 77 (1), 31–70. https://doi.org/10.1144/GSL.SP.1994.077.01.03.

Figueiredo, J.J.P., Hodgson, D.M., Flint, S.S., Kavanagh, J.P., 2010. Depositional environments and sequence stratigraphy of an exhumed permian mudstone-dominated submarine slope succession, karoo basin, South Africa. J. Sediment. Res. 80 (1), 97–118. https://doi.org/10.2110/jsr.2010.002.

Gong, X., Wang, Y.B., Yu, Y., 2022. Geochemical characteristics and hydrocarbon generation characteristics of Upper Paleozoic coal measures source rocks in Huanghua Depression, Bohai Bay Basin: case study of Dagang exploration area. Nat. Gas Geosci. 33 (6), 1013–1024. https://doi.org/10.11764/j.issn.1672-1926.2021.12.008 (in Chinese).

Guan, H.L., Wang, S.Y., Jiang, X.R., 2010. Characteristics and identification marks of burial dissolution pores in the reservoirs of the Changxing and Feixianguan formations in the Puguang gas field. Nat. Gas. Ind. 30 (3), 31–34. https://doi.org/10.1016/S1876-3804(11)60008-6.

Guo, B.W., Yu, F.S., Wang, Y.F., Li, H., Li, H.B., Wu, Z., 2022. Quantitative prediction of palaeo-uplift reservoir control and favorable reservoir formation zones in Lufeng Depression. Ager 6 (5), 426–437. https://doi.org/10.46690/ager.2022.05.07.

He, J.H., Ding, W.L., Zhang, J.C., Li, A., Zhao, W., Dai, P., 2016. Logging identification and characteristic analysis of marine–continental transitional organic-rich shale in the Carboniferous-Permian strata, Bohai Bay Basin. Mar. Petrol. Geol. 70, 273–293. https://doi.org/10.1016/j.marpetgeo.2015.12.006.

Hou, Z.S., Chen, S.Y., Yan, J.H., Fu, L.X., 2017. Sedimentary characteristics and control factors of Upper Palaeozoic in Dagang exploration area. J. Earth Sci. 42 (11), 2055–2068. https://doi.org/10.3799/dqkx.2017.131 (in Chinese).

Jia, J.L., Miao, C.S., Xie, W.Q., 2022. Terrestrial paleoclimate transition associated with continental weathering and drift during the Aptian–Albian of East Asia. GSA Bulletin 135 (1–2), 467–480. https://doi.org/10.1130/B36253.1.

Jia, J.L., Wu, Y.J., Miao, C.S., Fu, C.L., Xie, W.Q., Qin, J.Y., Wang, X.M., 2021. Tectonic controls on the sedimentation and thermal history of supra-detachment basins: a case study of the early Cretaceous Fuxin Basin, NE China. Tectonics 40 (5), e2020TC006535. https://doi.org/10.1029/2020TC006535.

Jiang, X.Q., Tian, N.X., Yin, J.X., Tao, C.Z., Wang, D.P., 2018. Global oil and gas distribution and exploration. Trend. Pet. Petrochem. Today 26 (6), 29–35. https://doi.org/10.3969/j.issn.1009-6809.2018.06.006.

Jin, Q., Song, G.Q., Wang, L., 2009. Generation models of carboniferous-permian coal-derived gas in shengli oilfield. Petrol. Explor. Dev. 36 (3), 358–364. https://doi.org/10.3321/j.issn:1000-0747.2009.03.011.

Jin, Z.J., 2023. Hydrocarbon accumulation and resources evaluation: recent advances and current challenges. Ager 8 (1). https://doi.org/10.46690/ager.2023.04.01.

Lee, H.T., Sun, L.C., 2016. Study on the relevant parameters for the single maceral compositions in thermal maturation. Environ. Earth Sci. 75 (2). https://doi.org/10.1007/s12665-015-4939-9.

Li, M.J., Wang, T.G., Shi, S.B., Zhu, L., Fang, R.H., 2014. Oil maturity assessment using maturity indicators based on methylated dibenzothiophenes. Petrol. Sci. 11 (2), 234–246. https://doi.org/10.1007/s12182-014-0336-3.

Li, R.X., Jin, K.L., Lehrmann, D.J., 2008. Hydrocarbon potential of pennsylvanian coal in Bohai gulf basin, eastern China, as revealed by hydrous pyrolysis. Int. J. Coal Geol. 73 (1), 88–97. https://doi.org/10.1016/j.coal.2007.07.006.

Li, Y., Tang, D.Z., Wu, P., Niu, X.L., Wang, K., Qiao, P., Wang, Z.S., 2016. Continuous unconventional natural gas accumulations of Carboniferous-Permian coal-bearing strata in the Linxing area, northeastern Ordos basin, China. J. Nat. Gas Sci. Eng. 36, 314–327. https://doi.org/10.1016/j.jngse.2016.10.037.

Li, Y., Wang, Z.S., Wu, P., Gao, X.D., Yu, Z.L., Yu, Y.H., 2019. Organic geochemistry of Upper Paleozoic source rocks in the eastern margin of the Ordos Basin, China: input and hydrocarbon generation potential. J. Petrol. Sci. Eng. 181, 106202. https://doi.org/10.1016/j.petrol.2019.106202.

Li, Y., Zhu, Y.M., Hao, F., Zou, H.Y., Guo, T.L., 2015. Thermal evolution and applications of aromatic hydrocarbons in highly mature coal-bearing source rocks of the Upper Triassic Xujiahe Formation in the northern Sichuan Basin. Sci. China Earth Sci. 58 (11), 1960–1969. https://doi.org/10.1007/s11430-015-5084-8.

Liao, Q.J., Yu, X.M., He, Y.M., Liu, X.J., 2003. The characteristics and resource potential of coal-bearing formations in Upper Paleozoic in Dagang Oilfield. Nat. Gas Geosci. 14 (4), 250–253. https://doi.org/10.11764/j.issn.1672-1926.2003.04.250.

Liu, B., Schieber, J., Mastalerz, M., 2020. Petrographic and micro-FTIR study of organic matter in the Upper Devonian New Albany Shale during thermal maturation; implications for kerogen transformation. AAPG Mem 120, 165–188. https://doi.org/10.1306/13672216M1213380.

Lou, D., Cao, Y.C., Peng, S.N., Fu, L.X., Li, H.J., Luo, R., Xu, J.J., Gong, S.H., 2022. Carboniferous–permian coaly source rock formation in north China: implications from geochemical characteristics and depositional environments. ACS Earth Space Chem. 6 (2), 444–454. https://doi.org/10.1021/acsearthspacechem.1c00414.

Mastalerz, M., Drobniak, A., Stankiewicz, A.B., 2018. Origin, properties, and implications of solid bitumen in source-rock reservoirs: a review. Int. J. Coal Geol. 195, 14–36. https://doi.org/10.1016/j.coal.2018.05.013.

Meng, Q., Wang, X.F., Liao, Y.H., Lei, Y.H., Yin, J.T., Liu, P., Shi, B.G., 2021. The effect of slight to moderate biodegradation on the shale soluble organic matter composition of the upper triassic Yanchang formation, Ordos Basin, China. Mar. Petrol. Geol. 128, 105021. https://doi.org/10.1016/j.marpetgeo.2021.105021.

Michelsen, J.K., Khorasani, G.K., 1990. Monitoring chemical alterations of individual oil-prone macerals by means of microscopical fluorescence spectrometry combined with multivariate data analysis. Org. Geochem. 15 (2), 179–192. https://doi.org/10.1016/0146-6380(90)90082-B.

Misch, D., Sachsenhofer, R.F., Bechtel, A., Gratzer, R., Gross, D., Makogon, V., 2015. Oil/gas-source rock correlations in the Dniepr-Donets Basin (Ukraine): new insights into the petroleum system. Mar. Petrol. Geol. 67, 720–742. https://doi.org/10.1016/j.marpetgeo.2015.07.002.

Misch, D., Gross, D., Hawranek, G., Horsfield, B., Klaver, J., Mendez-Martin, F., Urai, J.L., Vranjes-Wessely, S., Sachsenhofer, R.F., Schmatz, J., Li, J., Zou, C., 2019. Solid bitumen in shales: petrographic characteristics and implications for reservoir characterization. Int. J. Coal Geol. 205, 14–31. https://doi.org/10.1016/j.coal.2019.02.012.

Petersen, H.I., Andsbjerg, J., Bojesen-Koefoed, J.A., Nytoft, H.P., 2000. Coal-generated oil: source rock evaluation and petroleum geochemistry of the lulita oilfield, Danish North Sea. J. Petrol. Geol. 23 (1), 55–90. https://doi.org/10.1111/j.1747-5457.2000.tb00484.x.

Qi, Y., Ju, Y.W., Tan, J.Q., Bowen, L., Cai, C.F., Yu, K., Zhu, H.J., Huang, C., Zhang, W.L., 2020. Organic matter provenance and depositional environment of marine-to-continental mudstones and coals in eastern Ordos Basin, China—evidence from molecular geochemistry and petrology. Int. J. Coal Geol. 217, 103345. https://doi.org/10.1016/j.coal.2019.103345.

Qu, X.R., Zhu, Y.M., Li, W., Tang, X., Zhang, H., 2018. Evaluation of hydrocarbons generated from the permo-carboniferous source rocks in Huanghua depression of the Bohai Bay Basin, China. Energy Explor. Exploit. 36 (5), 1229–1244. https://doi.org/10.1177/0144598718755465.

Radke, M., Welte, D.H., Willsch, H., 1982. Geochemical study on a well in the Western Canada Basin: relation of the aromatic distribution pattern to maturity of organic matter. Geochem. Cosmochim. Acta 46 (1), 1–10. https://doi.org/10.1016/0016-7037(82)90285-X.

Radke, M., Welte, D.H., Willsch, H., 1986. Maturity parameters based on aromatic hydrocarbons: influence of the organic matter type. Org. Geochem. 10 (1), 51–63. https://doi.org/10.1016/0146-6380(86)90008-2.

Rangel, A., Moldowan, J.M., Nino, C., Parra, P., Giraldo, B.N., 2002. Umir Formation: organic geochemical and stratigraphic assessment as cosource for Middle Magdalena Basin oil, Colombia. AAPG Bull. 86 (12), 2069–2085. https://doi.org/10.1306/61EEDE04-173E-11D7-8645000102C1865D.

Schenk, H.J., Di Primio, R., Horsfield, B., 1997. The conversion of oil into gas in petroleum reservoirs. Part 1: comparative kinetic investigation of gas generation from crude oils of lacustrine, marine and fluviodeltaic origin by programmed-temperature closed-system pyrolysis. Org. Geochem. 26 (7–8), 467–481. https://doi.org/10.1016/S0146-6380(97)00024-7.

Tewari, R.C., Khan, Z.A., 2015. Origin of banded structure and coal lithotype cycles in Kargali coal seam of East Bokaro sub-basin, Jharkhand, India: environmental implications. J. Earth Syst. Sci. 124 (3), 643–654. https://doi.org/10.1007/s12040-015-0553-1.

Van Krevelen, D.W., 1993. Coal: Typology-Physics-Chemistry-Constitution. Elsevier Science Publishers, Netherlands Amsterdam. https://doi.org/10.5860/choice.31-3793.

Wang, C.J., Zhang, H., Li, S.Y., Wen, L., 2018. Maturity parameters selection and applicable range analysis of organic matter based on molecular markers. Bulletin of Geological Science and Technology 37 (4), 202–211. https://doi.org/10.19509/j.cnki.dzkq.2018.0427 (in Chinese).

Wang, D.D., Shao, L.Y., Li, Z.X., Li, M.P., Lv, D.W., Liu, H.Y., 2016. Hydrocarbon generation characteristics, reserving performance and preservation conditions of continental coal measure shale gas: a case study of Mid-Jurassic shale gas in the Yan'an Formation, Ordos Basin. J. Pet. Sci. Eng. 145, 609–628. https://doi.org/10.1016/j.petrol.2016.06.031.

Wang, W.Y., Pang, X.Q., Chen, Z.X., Chen, D.X., Ma, X.H., Zhu, W.P., Zheng, T.Y., Wu, K.L., Zhang, K., Ma, K.Y., 2020. Improved methods for determining effective

sandstone reservoirs and evaluating hydrocarbon enrichment in petroliferous basins. Appl. Energy 261, 114457. https://doi.org/10.1016/j.apenergy.2019.114457.

Wang, W.Y., Pang, X.Q., Wang, Y.P., Chen, Z.X., Li, C.R., Ma, X.H., 2022. Hydrocarbon expulsion model and resource potential evaluation of high-maturity marine source rocks in deep basins: example from the Ediacaran microbial dolomite in the Sichuan Basin, China. Petrol. Sci. 19 (6), 2618–2630. https://doi.org/10.1016/j.petsci.2022.11.018.

Xin, Y.P., Qin, J.Z., Zheng, L.J., Qiu, N.S., 2010. Secondary hydrocarbon generation potential of marine shale source rocks in thermal modeling. Geosci. 24 (6), 1079–1084. https://doi.org/10.3969/j.issn.1000-8527.2010.06.008.

Xu, J.J., Lou, D., Jin, Q., Fu, L.X., Cheng, F., Zhou, S.H., Wang, X.H., Liang, C., Li, F.L., 2021. Discriminating hydrocarbon generation potential of coaly source rocks and their contribution: a case study from the Upper Paleozoic of Bohai Bay Basin, China. Front. Earth Sci. 15 (4), 876–891. https://doi.org/10.1007/s11707-021-0908-7.

Xu, J.J., Jin, Q., 2020a. Hydrocarbon generation from Carboniferous-Permian coaly source rocks in the Huanghua depression under different geological processes. Petrol. Sci. 17 (6), 1540–1555. https://doi.org/10.1007/s12182-020-00513-2.

Xu, J.J., Jin, Q., 2020b. Hydrocarbon potential and polycyclic aromatic compounds differences of Carboniferous-Permian coaly source rocks, Bohai Bay Basin: an implication for different sources of gas condensate and oils. J. Pet. Sci. Eng. 195, 107899. https://doi.org/10.1016/j.petrol.2020.107899.

Yan, W.Q., Li, J.N., Sun, Y.H., 2020. Burial history of Upper Paleozoic and prediction of favorable hydrocarbon-generating areas in Huanghua. Miner. Explor. 11 (8), 1690–1696. https://doi.org/10.3969/j.issn.1674-7801.2020.08.018.

Yu, K., Ju, Y.W., Qian, J., Qu, Z.H., Shao, C.J., Yu, K.L., Shi, Y., 2018. Burial and thermal evolution of coal-bearing strata and its mechanisms in the southern North China Basin since the late Paleozoic. Int. J. Coal Geol. 198, 100–115. https://doi.org/10.1016/j.coal.2018.09.007.

Zhang, J.N., Zhou, J.S., Xiao, D.Q., Han, G.M., Zhao, M., Fu, L.X., Li, H.J., Lou, D., 2019. Control of the mesozoic tectonic movement on the hydrocarbon generation and evolution of upper paleozoic coal-measure source rocks in the Huanghua depression, Bohai Bay Basin. NGI 39 (9), 1–10. https://doi.org/10.3787/j.issn.1000-0976.2019.09.001.

Zhao, W.Z., Wang, Z.Y., Wang, H.J., Li, Y.X., Hu, G.Y., Zhao, C.Y., 2011. Further discussion on the connotation and significance of the natural gas relaying generation model from organic materials. Petrol. Explor. Dev. 38 (2), 129–135. https://doi.org/10.1016/S1876-3804(11)60021-9.

Zhao, X.Z., Zhou, L.H., Pu, X.G., Jiang, W.Y., Jin, F.M., Xiao, D.Q., Han, W.Z., Zhang, W., Shi, Z.M., Li, Y., 2018. Hydrocarbon-generating potential of the upper paleozoic section of the Huanghua depression, Bohai Bay Basin, China. Energy Fuel. 32 (12), 12351–12364. https://doi.org/10.1021/acs.energyfuels.8b03159.

Zhao, X.Z., Pu, X.G., Jiang, W.Y., Zhou, L.H., Jin, F.M., Xiao, D.Q., Fu, L.X., Li, H.J., 2019. An exploration breakthrough in paleozoic petroleum system of Huanghua depression in Dagang oilfield and its significance, north China. Petrol. Explor. Dev. 46 (4), 651–663. https://doi.org/10.1016/S1876-3804(19)60224-7.

Zheng, L.J., Qin, J.Z., He, S., Li, G.Y., Li, Z.M., 2009. Preliminary study of formation porosity thermocompression simulation experiment of hydrocarbon generation and expulsion. Petrol Geo & Exper 31 (3), 296–302+306. https://doi.org/10.3969/j.issn.1001-6112.2009.03.017 (in Chinese).

Zhu, Y.M., Qin, Y., Sang, S.X., Chen, S.B., Lan, X.D., 2010. Hydrocarbon generation evolution of permo-carboniferous rocks of the Bohai Bay Basin in China. Acta Geol Sin-Engl 84 (2), 370–381. https://doi.org/10.1111/j.1755-6724.2010.00163.x.